Ytterbium-ion pairs in Yb:$CsCdBr_3$; ion-ion interaction and the electronic ground state investigated by electron paramagnetic resonance spectroscopy

2001 J. Phys.: Condens. Matter 13 4567

(http://iopscience.iop.org/0953-8984/13/20/317)

INSTITUTE OF PHYSICS PUBLISHING JOURNAL OF PHYSICS: CONDENSED MATTER

J. Phys.: Condens. Matter **13** (2001) 4567–4578 www.iop.org/Journals/cm PII: S0953-8984(01)20309-9

Ytterbium-ion pairs in Yb:$CsCdBr_3$; ion–ion interaction and the electronic ground state investigated by electron paramagnetic resonance spectroscopy

V Mehta[1] **and D Gourier**[2]

Laboratoire de Chimie Appliquée de l'Etat Solide, Ecole Nationale Supérieure de Chimie de Paris (ENSCP), UMR CNRS 7574, 11 rue Pierre et Marie Curie, 75231 Paris Cédex 05, France

E-mail: gourierd@ext.jussieu.fr (D Gourier)

Received 22 December 2000, in final form 7 March 2001

Abstract

Electron paramagnetic resonance spectra of Yb^{3+} ions in the optically bistable compound Yb:$CsCdBr_3$ are presented. The features observed are assigned to the symmetrically coupled pair complexes of the type Yb^{3+}–V_{Cd}–Yb^{3+} (V_{Cd} being a cadmium vacancy) whose axis is parallel to the crystallographic *c*-axis. There are no asymmetric pairs of the type Yb^{3+}–Yb^{3+}–V_{Cd}. It is shown that simulation of the spectra is possible only if an exchange interaction is taken into account in the spin Hamiltonian. The value of $J = -0.0016\ cm^{-1}$ shows that the exchange interaction is antiferromagnetic but extremely weak. It is also found that there is a significant relaxation (about 12%) of Yb^{3+} ions toward the Cd vacancy. From the experimental *g*-tensor values, it is established that the lower ground state of Yb^{3+} ions in $CsCdBr_3$ is mainly composed of $4f_\phi$ (63%) and $4f_\delta$ (32%) ytterbium orbitals. It has been previously proposed that optical bistability is due to asymmetric pairs of the type Yb^{3+}–Yb^{3+}–V_{Cd}. On the basis of the present work, this now appears unlikely.

1. Introduction

The presence of two stable transmission or emission intensity values for a single input intensity, outside an optical cavity, a phenomenon known as intrinsic optical bistability (IOB), was demonstrated for the first time in 1994 in a rare-earth dimer compound $Cs_3Y_2Br_9$:10% Yb^{3+} by Hehlen *et al* [1]. This experimental observation of all-optical switching originating from rare-earth-ion pairs was later extended to the isostructural systems $Cs_3Lu_2Br_9$:10% Yb^{3+} and $Cs_3Yb_2Br_9$ [2] and more recently to a quasi-one-dimensional compound $CsCdBr_3$:1% Yb^{3+} [3]. Studies on these materials suggest that non-linearities mediated by local field effects may cause hysteresis of near-infrared and cooperative upconversion luminescence, with the

[1] Present address: Department of Physics, Kalindi College, University of Delhi, East Patel Nagar, New Delhi-110008, India.

[2] Author to whom any correspondence should be addressed.

0953-8984/01/204567+12$30.00

possibility of optical switching between the two states. These non-linearities arise from strong ion–ion coupling within well-isolated dimers. Because of the potential applications of IOB in communications and optical computing, a precise knowledge of ion–ion interactions in such pairs is of fundamental interest for understanding the IOB mechanism.

$CsCdBr_3$ adopts a hexagonal structure with space group $P6_3/mmc$ (D^4_{6h}), and belongs to the AMX_3 series of host materials where A is a monovalent metal, M a divalent metal and X a halide. The basic lattice is built of linear arrays of face-sharing $(CdBr_6)^{4-}$ octahedra parallel to the crystallographic c-axis, the charge being balanced by Cs^+ ions occupying sites between the chains. The point symmetries of the cation sites are D_{3h} for Cs^+ and D_{3d} for Cd^{2+}. The distance between the Cd^{2+} ions along a chain is much smaller than the separation between the chains, which gives this structure an essentially one-dimensional character. In addition, the most prominent feature of these crystals is that when rare-earth (RE^{3+}) ions such as Yb^{3+} are incorporated at the Cd^{2+} lattice position, they appear exclusively as ion pair centres, even at low dopant concentration. This tendency of RE^{3+} ions to form pairs is the consequence of the charge compensation. The main RE centre is a symmetric in-chain pair complex of the type [RE^{3+}–V_{Cd}–RE^{3+}] and was identified by McPherson and Henling by means of EPR experiments on Gd^{3+} [4]. Each individual RE^{3+} ion of the pair has C_{3v} site symmetry. The distance R between the ions attracted by the Cd^{2+} vacancy reduced from the lattice constant value $c = 6.722$ Å to around 6.0 Å. A minority Cr^{3+}–(Cs^+ vacancy) complex of lower symmetry (C_S) was also identified by means of EPR in a chromium-doped compound [5]. Subsequent laser spectroscopic studies on $CsCdBr_3$ doped with Nd^{3+} [6], Er^{3+}[7] and Pr^{3+}[8] suggested the presence of an asymmetric in-chain [RE^{3+}–RE^{3+}–V_{Cd}] complex in small quantities. In this complex, the two RE^{3+} ions have non-equivalent crystal fields and the distance R between them is around 3.4 Å. The predominance of these pair centres, in which the RE^{3+} ions are separated by a small distance, makes $CsCdBr_3$ an ideal host for studying energy-transfer processes, upconversion and cross-relaxation mechanisms for application in laser systems, and also detailed RE^{3+}–RE^{3+} pair interactions in well-defined and relatively simple crystalline environments. Although the optical properties of $CsCdBr_3$ activated by different RE^{3+} ions have been widely studied [6–13], the identification of optical lines with specific impurity centres is still of more or less hypothetical character, and the cause of there being more 4f–4f transitions than expected in the absorption or emission spectra is still not clear [3].

In a recent comprehensive paper, Malkin *et al* [14] reported EPR and optical spectra of Yb^{3+}–V_{Cd}–Yb^{3+} centres in $CsCdBr_3$, and explained the crystal-field energies in terms of mixing of the ground-state configuration with ligand-to-metal charge-transfer configurations. These authors interpreted the EPR spectra of Yb^{3+} pairs in terms of a spin Hamiltonian in which the ion–ion interaction is of the magnetic dipole–dipole type. The isotropic interaction J was not taken into consideration. This reasonable assumption is supported by the fact that there is no evidence of such interaction in the optical spectra [6–13], which implies $J \ll 1\ \mathrm{cm}^{-1}$. However, from the examination of the EPR spectra reported in reference [14], it appears evident that the calculated hyperfine patterns of Yb^{3+} pairs are different from the experimental ones. A possible explanation for this discrepancy could be the presence of an isotropic exchange interaction, which was not taken into account in the spin Hamiltonian. Recently, by using EPR and high-resolution optical spectroscopy, we have demonstrated that ground-state ferromagnetic exchange interactions are responsible for the extra optical lines for neodymium-doped $LiYF_4$ and YVO_4 laser crystals [15]. In the case of ytterbium in $CsCdBr_3$, the separation between two adjacent hyperfine transitions for a given value m_1 of the nuclear spin component of one ion (^{171}Yb or ^{173}Yb) of the pair should be of the order of $4D - 2J$, where D is the dipole–dipole interaction. If J is not too small compared to D, this correction should modify the shape of the hyperfine pattern for pairs and could explain the discrepancy

between experimental and calculated spectra in reference [14]. In the present work we report a detailed EPR study of Yb^{3+} pairs in $CsCdBr_3$, with a view to identifying the respective effects of dipole–dipole and exchange interactions

2. Experimental procedure

$CsCdBr_3$ single crystals of 1.3% ytterbium concentration were grown by the Bridgman method. EPR spectra were recorded on a Bruker ESP 300e spectrometer equipped with a TE 102 rectangular cavity and a variable-temperature accessory from Oxford Instruments. The crystal was mounted on a small Perspex sample holder to allow its orientation to be varied with respect to the magnetic field. The microwave frequency was measured with a Systron Donner frequency counter. Typical measurements were made at 7 K with a microwave power of 20 mW and a frequency of approximately 9.5 GHz.

3. Results

The principal EPR signals, observed in the range 210–320 mT, are shown in figure 1 for the external magnetic field $\boldsymbol{B}$ both parallel and perpendicular to the crystallographic c-axis. In addition, weaker EPR signals are observed at half-fields ($\sim$130 mT) when $\boldsymbol{B}$ is away from the symmetry axis. Figure 2(a) shows such a half-field resonance (HFR) spectrum at $\theta = 45^\circ$ where θ is the angle between the direction of the magnetic field $\boldsymbol{B}$ and the c-axis. The angular dependence of the principal as well as HFR spectra in the a–c (or b–c) and a–b crystallographic planes shows that the resonance lines have axial symmetry about the trigonal c-axis. The complexity of the spectra is due to the fact that ytterbium has one even isotope of natural abundance 69% and two odd isotopes which give rise to hyperfine structures, (^{171}Yb, $I = 1/2$, 14.4% and ^{173}Yb, $I = 5/2$, 16.6%). All of the spectral features can be accurately described by assigning the resonance lines to the symmetric pairs of the type ^{even}Yb–V_{Cd}–^{even}Yb, ^{171}Yb–V_{Cd}–^{even}Yb and ^{173}Yb–V_{Cd}–^{even}Yb, with Yb^{3+} ions at identical crystallographic sites [14].

The Hamiltonian for a pair of identical interacting ions 1 and 2 can be written as

$$H = H_1 + H_2 + V \tag{1}$$

where H_1 and H_2 are the individual ion Hamiltonians and V represents the pairing effect. H_1 and H_2 for single Yb^{3+} ions at Cd^{2+} sites of the host include the free-ion Hamiltonian H_0 and the crystal-field Hamiltonian H_{cf}. The component H_0 contains electron–electron and spin–orbit interaction terms and gives the two $^{2S+1}L_J$ multiplets of Yb^{3+}, the ground state $^2F_{7/2}$ and the only excited state $^2F_{5/2}$, separated by around 10 000 cm^{-1}. The crystal-field term H_{cf} lifts the $2J + 1$ degeneracy of the $^{2S+1}L_J$ states, making them doubly degenerate states, referred to as Kramers doublets (KDs). The residual degeneracy of a KD can only be removed by an external magnetic field. At liquid helium temperature, only the lowest doublet is populated and, therefore, we can attribute an effective spin $S = 1/2$ to it. The EPR spectrum of an isolated ion can thus be treated by an effective spin Hamiltonian consisting of electronic Zeeman terms and the additional nuclear hyperfine terms for odd isotopes [14].

The pairing term V can be written as the interaction between two identical effective spins S_1 and S_2 of the lowest ground-state Kramers doublet of the two Yb^{3+} ions:

$$V_{eff} = -2J\vec{S}_1 \cdot \vec{S}_2 + \frac{\beta^2}{R^3}\left[-2g_\parallel^2(S_{1z}S_{2z}) + \frac{g_\perp^2}{2}(S_{1+}S_{2-} + S_{1-}S_{2+})\right]. \tag{2}$$

The first and the second terms in this expression are the isotropic Heisenberg exchange and anisotropic dipolar contributions respectively, J is the scalar exchange interaction and R is the

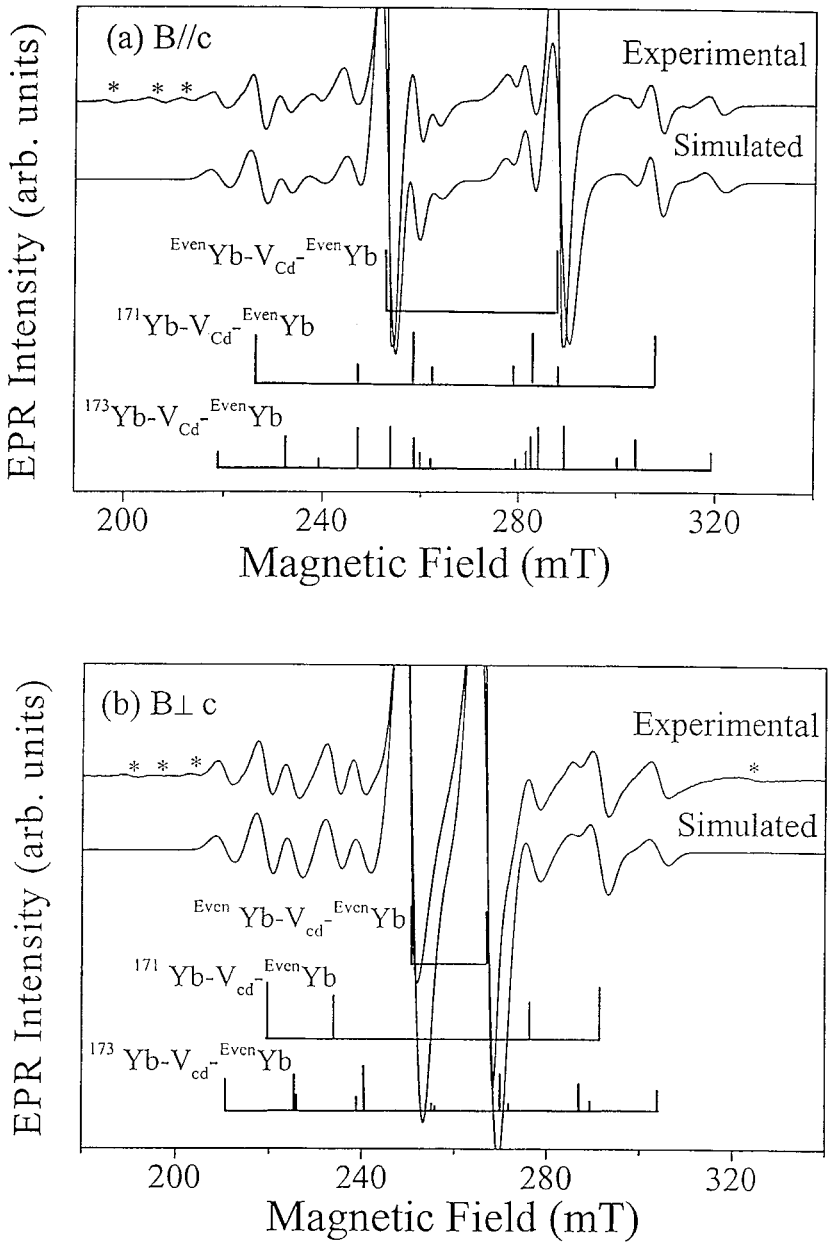

Figure 1. Experimental and simulated EPR spectra of 1.3% Yb^{3+}:$CsCdBr_3$ at 7 K with (a) $\boldsymbol{B} \parallel \boldsymbol{c}$ and (b) $\boldsymbol{B} \perp \boldsymbol{c}$. The stars indicate very weak EPR lines due to non-axial Yb^{3+} centres.

RE–RE distance. The z-axis (RE–RE axis) is parallel to the crystal symmetry axis. Two-centre or direct exchange and multicentre or superexchange processes involving the ligands can both contribute to J [16]. The isotropic interaction produces a splitting of magnitude J between the singlet spin state and the centre of gravity of the triplet spin states. The anisotropic term produces splittings within the triplet levels without altering the centre of gravity. The pure magnetic dipole–dipole expression has been used for the anisotropic dipolar interaction in

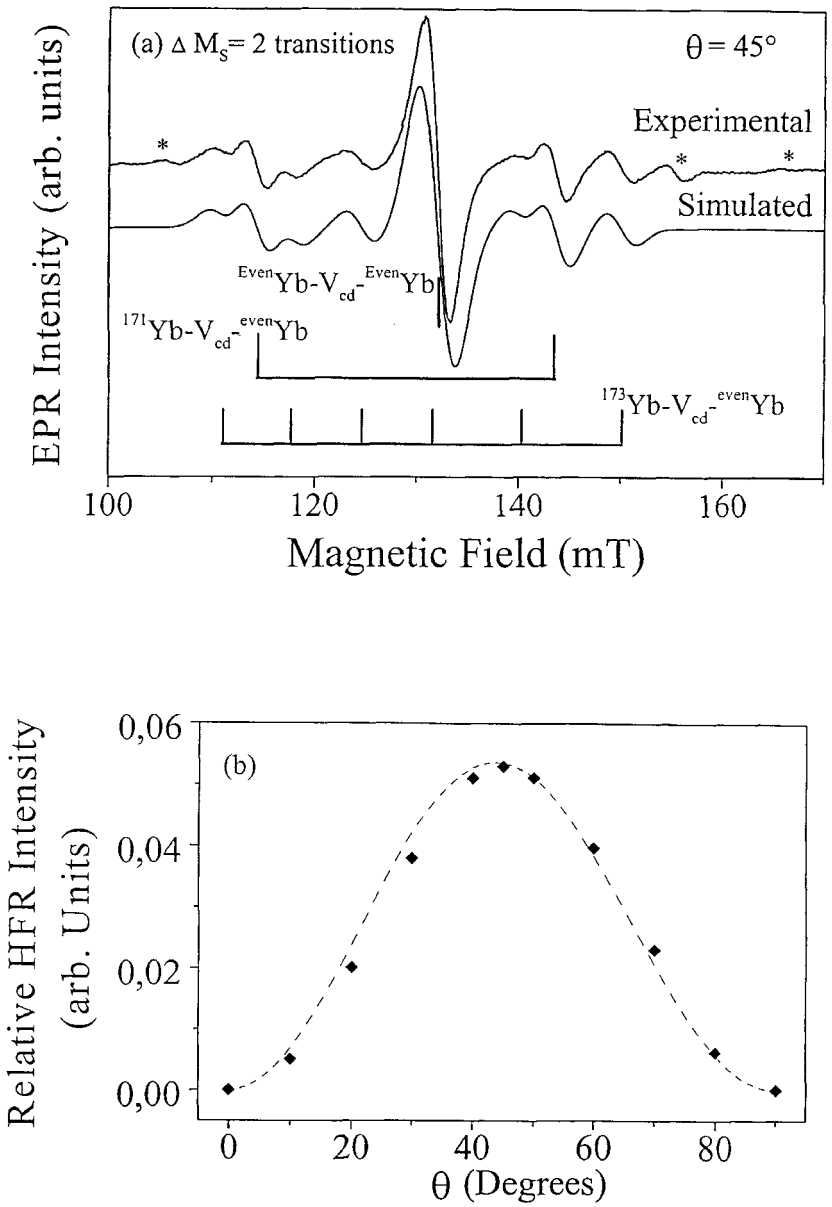

Figure 2. (a) Experimental and simulated half-field resonance (HFR) spectra for $\boldsymbol{B}$ making an angle of $\theta = 45^\circ$ with the c-axis. The stars indicate very weak EPR lines due to non-axial Yb^{3+} centres. (b) The measured (♦) and calculated (broken curve) relative intensity of the HFR line due to even–even Yb pairs as a function of θ.

equation (2) as in reference [14] because the distance R between the two Yb^{3+} ions of a pair is relatively large compared to the ion size, so the multipole expansion of the magnetic spin–spin interaction should converge sufficiently to give a leading term of the magnetic dipole–dipole type. It should be mentioned that the exchange interactions between paramagnetic ions with unquenched orbital momentum, which is the case with rare-earth ions, are generally considered

to be rather complex [17] and to deviate from the well-known Heisenberg form. Various other terms like antisymmetric exchange, anisotropic bilinear exchange and biquadratic exchange involving other mechanisms of spin–spin interaction such as electric multipole interactions and virtual phonon exchange may also contribute to the interaction term V_{eff} [17, 18]. However, we have recently shown that the high-resolution optical spectra of Nd^{3+} pairs in Nd:YVO_4 and Nd:$YLiF_4$ can be accurately interpreted by considering only isotropic Heisenberg exchange interactions [15]. In this work also, the use of expression (2) in its present form will be justified *a posteriori* in relation to the experimental results.

The total effective spin Hamiltonian appropriate for describing the EPR spectra of a pair of interacting even–even isotopes of Yb can thus be written as

$$H_{eff} = g_{\parallel}\beta B_z(S_{1z} + S_{2z}) + g_{\perp}\beta\left[B_x(S_{1x} + S_{2x}) + B_y(S_{1y} + S_{2y})\right] + \left[\frac{\beta^2}{R^3}(-2g_{\parallel}^2) - 2J\right](S_{1z}S_{2z}) + \frac{1}{2}\left[\frac{\beta^2}{R^3}(g_{\perp}^2) - 2J\right](S_{1+}S_{2-} + S_{1-}S_{2+}). \tag{3}$$

When the external magnetic field $\boldsymbol{B}$ is at an angle θ with the symmetry axis, we can write $B_z = B\cos\theta$, $B_x = B\sin\theta$ and $B_y = 0$. The anisotropy of the g-tensor means that the electron spin will not, in general, be parallel to $\boldsymbol{B}$. Choosing a new coordinate system (x', y', z') where each electronic spin is diagonal along z' and the $0z'$-axis makes an angle ϕ with $0z$, the spin Hamiltonian in equation (3) transforms to

$$H_{eff} = g(\theta)B(S_{1z'} + S_{2z'}) + (4D_1 - 2J)(S_{1z'}S_{2z'}) + (D_2 - J)(S_{1+'}S_{2-'} + S_{1-'}S_{2+'}) + D_3(S_{1+'}S_{2+'} + S_{1-'}S_{2-'}) + D_4(S_{1+'}S_{2z'} + S_{1-'}S_{2z'} + S_{1z'}S_{2+'} + S_{1z'}S_{2-'}) \tag{4}$$

where $g_{\parallel}\cos\theta = g\cos\phi$, $g_{\perp}\sin\theta = g\sin\phi$ and $g^2(\theta) = g_{\parallel}^2\cos^2\theta + g_{\perp}^2\sin^2\theta$ in axial symmetry. The dipolar terms D_i ($i = 1$ to 4) in equation (4) are defined as

$$\begin{aligned} D_1 &= \frac{\beta^2}{4R^3}\left[(g_{\perp}^4\sin^2\theta - 2g_{\parallel}^4\cos^2\theta)/g^2(\theta)\right] \\ D_2 &= \frac{\beta^2}{4R^3}\left[\left\{2g_{\parallel}^2(1 - 2\sin^2\theta) + g_{\perp}^2\sin^2\theta\right\}g_{\perp}^2/g^2(\theta)\right] \\ D_3 &= -\frac{\beta^2}{4R^3}\left[g_{\perp}^2(g_{\perp}^2 + 2g_{\parallel}^2)\sin^2\theta/g^2(\theta)\right] \\ D_4 &= \frac{\beta^2}{4R^3}\left[(g_{\perp}^2 + 2g_{\parallel}^2)g_{\parallel}g_{\perp}\sin\theta\cos\theta/g^2(\theta)\right]. \end{aligned} \tag{5}$$

The basis states of the form $|\pm\frac{1}{2}, \pm\frac{1}{2}\rangle = |M_{S_1}\rangle|M_{S_2}\rangle$ are used to solve this Hamiltonian, $M_{S_i} = \pm\frac{1}{2}$ being the z-projection of the effective spin S on ion i. From the eigenstates of H_{eff}, we expect two $\Delta M_S = \pm 1$ transitions at magnetic fields

$$B_{\pm} = B_0\left[1 \pm \frac{(-2D_1 + D_2)}{g\beta B_0} - \frac{(2D_4^2 + \frac{1}{2}D_3^2)}{(g\beta B_0)^2}\right] \tag{6}$$

where B_0 is the centre resonance field. The corresponding relative intensities, calculated up to first order in the perturbation, are

$$\frac{1}{2}\left(1 \pm \frac{D_3}{g\beta B_0}\right). \tag{7}$$

A single $\Delta M_S = \pm 2$ forbidden half-field transition is also expected at

$$B_F = B_0\left[\frac{1}{2} - \frac{(4D_4^2 + D_3^2)}{2(g\beta B_0)^2}\right] \tag{8}$$

with relative intensity $4D_4^2/(g\beta B_0)^2$ up to second order in the perturbation.

Figure 3 shows the observed angular variation of the low-field ($\boldsymbol{B}_-$) and high-field ($\boldsymbol{B}_+$) allowed $\Delta M_S = \pm 1$ transitions due to interacting even–even isotopes of Yb in the a–c (or b–c) crystallographic plane. The two transitions cross over at an angle θ between 50° and 55°. The measured relative intensity of the corresponding HFR line due to even–even Yb pairs as a function of θ is shown in figure 2(b). Since the intensity depends on the square of the dipolar parameter D_4, i.e. on $\sin^2 2\theta$ (see equation (5)), it is greatest when the magnetic field is at 45° to the z-axis and at its minimum along the principal axes.

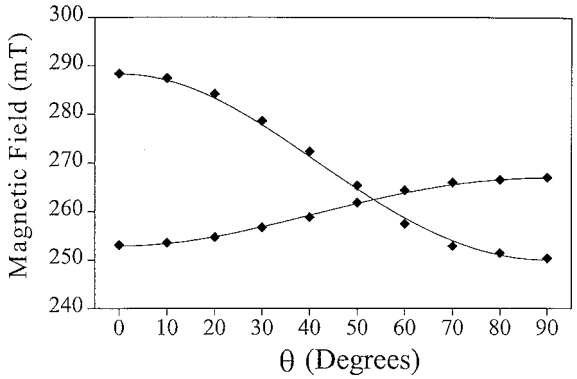

Figure 3. Experimental (♦) and calculated (solid curves) angular variations of the two allowed $\Delta M_S = \pm 1$ transitions due to interacting even–even Yb pairs in the a–c (or b–c) crystallographic plane.

When ion 1 has a nuclear spin I_1 (for example for the pairs of the type ^{171}Yb–V_{Cd}–^{even}Yb or ^{173}Yb–V_{Cd}–^{even}Yb), the hyperfine terms $A_\parallel(S_{1z}I_{1z}) + \frac{1}{2}A_\perp(S_{1+}I_{1-} + S_{1-}I_{1+})$ are included in the effective spin Hamiltonian of equation (3). As before, we again choose a new coordinate system (x'', y'', z'') where the nuclear spin is diagonal along z'' and $0z''$ and makes an angle ψ with $0z$. The following hyperfine terms are thus added to equation (4):

$$K(\theta)S_{1z'}I_{1z''} + \frac{A_\parallel A_\perp}{K(\theta)}S_{1x'}I_{1x''} + A_\perp S_{1y'}I_{1y''} + R(\theta)S_{1x'}I_{1z''}$$

where

$$A_\parallel g_\parallel \cos\theta = Kg\cos\psi \qquad A_\perp g_\perp \sin\theta = Kg\sin\psi$$
$$K^2(\theta)g^2(\theta) = A_\parallel^2 g_\parallel^2 \cos^2\theta + A_\perp^2 g_\perp^2 \sin^2\theta$$
$$R(\theta) = (A_\perp^2 - A_\parallel^2)g_\parallel g_\perp \sin\theta\cos\theta/K(\theta)g^2(\theta).$$

For a particular $m_1 = \langle I_z\rangle$ state, the $\Delta M_S = \pm 1$ transitions can now be shown to occur at the fields (the theoretical treatment is similar to that outlined in [18])

$$B_{1,2} = B_0\Bigg[1 \mp \frac{2D_1'}{g\beta B_0} - \frac{(\frac{1}{2}Km_1 \mp \varphi)}{g\beta B_0} - \frac{(2D_4^2 + \frac{1}{2}D_3^2)}{(g\beta B_0)^2} - \frac{\frac{1}{2}R^2m_1^2(b_1^2 + a_2^2)}{(g\beta B_0)^2}$$
$$\mp \frac{2D_4Rm_1(1+ab)}{(g\beta B_0)^2} - \frac{A_\perp^2}{4}\left(\frac{A_\perp^2 + K^2}{K^2}\right)\frac{\left[I(I+1) - m_1^2\right](b_1^2 + a_2^2)}{(g\beta B_0)^2}\Bigg] \qquad (9a)$$

$$B_{3,4} = B_0\Bigg[1 \mp \frac{2D_1'}{g\beta B_0} - \frac{(\frac{1}{2}Km_1 \pm \varphi)}{g\beta B_0} - \frac{(2D_4^2 + \frac{1}{2}D_3^2)}{(g\beta B_0)^2} - \frac{\frac{1}{2}R^2m_1^2(a_3^2 + b_4^2)}{(g\beta B_0)^2}$$
$$\mp \frac{2D_4Rm_1(1-ab)}{(g\beta B_0)^2} - \frac{A_\perp^2}{4}\left(\frac{A_\perp^2 + K^2}{K^2}\right)\frac{[I(I+1) - m_1^2](a_3^2 + b_4^2)}{(g\beta B_0)^2}\Bigg]. \qquad (9b)$$

Their relative intensities calculated up to second order are respectively

$$\frac{1}{4}(a+b)^2\left(1 \pm \frac{D_3}{g\beta B_0}\right) \tag{10a}$$

and

$$\frac{1}{4}(a-b)^2\left(1 \mp \frac{D_3}{g\beta B_0}\right). \tag{10b}$$

The parameters D_1' and D_2' are defined as $D_1' = D_1 - J/2$ and $D_2' = D_2 - J$ and the other parameters φ, a and b in (9) and (10) are given as

$$\varphi = (D_2'^2 + \tfrac{1}{4}K^2m_1^2)^{1/2}$$

$$a = \frac{D_2'}{[D_2'^2 + (\varphi - \frac{1}{2}Km_1)^2]^{1/2}} = \frac{D_2'}{f_1}$$

and

$$b = \frac{\varphi - \frac{1}{2}Km_1}{f_1}.$$

We expect $4(2I+1)$ allowed $\Delta M_S = \pm 1$ transitions when one of the ytterbium isotopes of a pair has a nuclear magnetic moment. Thus for ^{171}Yb–V_{Cd}–^{even}Yb pairs there will be eight allowed transitions while for ^{173}Yb–V_{Cd}–^{even}Yb pairs there will be 24 allowed transitions.

The forbidden $\Delta M_S = \pm 2$ transitions are now expected at the magnetic fields

$$B_F(m_1) = B_0\left[\frac{1}{2} - \frac{Km_1}{2g\beta B_0} - \frac{(4D_4^2 + D_3^2)}{2(g\beta B_0)^2} - \frac{R^2m_1^2}{(2g\beta B_0)^2} - \frac{A_\perp^2}{4}\left(\frac{A_\perp^2 + K^2}{K^2}\right)\frac{\left[I(I+1) - m_1^2\right]}{(g\beta B_0)^2}\right] \tag{11}$$

with relative intensity $4D_4^2/(g\beta B_0)^2$.

The spin-Hamiltonian parameters determined by fitting the experimental spectra with their computer simulations are reported in table 1. Simulated spectra, shown in figure 1, are obtained by assuming Gaussian line-shape functions. The line positions are calculated from equations (6) and (9) and their relative intensities from equations (7) and (10). The agreement is excellent, with deviations of around 0.4% compared to the overall splittings. The good quality of this fitting shows that it is not necessary to take into account pairs of the type ^{173}Yb–V_{Cd}–^{173}Yb, ^{171}Yb–V_{Cd}–^{171}Yb and ^{171}Yb–V_{Cd}– ^{173}Yb, with natural abundances 2%, 2.8% and 4.8%, respectively. The number of hyperfine lines is so large in these cases that their amplitudes are completely negligible. The positions and intensities of the most important lines are also depicted as a stick diagram in figure 1. In the case of ^{173}Yb–V_{Cd}–^{even}Yb pairs, eight very weak resonance lines in the field range 252–284 mT are not shown in the stick diagram of figure 1(a) for $\boldsymbol{B} \parallel \boldsymbol{c}$. For $\boldsymbol{B} \perp \boldsymbol{c}$, four resonance lines in the case of ^{171}Yb–V_{Cd}–^{even}Yb pairs and twelve resonance lines in the case of ^{173}Yb–V_{Cd}–^{even}Yb pairs, of varying intensities, all coinciding

Table 1. Spin-Hamiltonian parameters of the Yb^{3+}–V_{Cd}–Yb^{3+} complexes in 1.3% Yb:$CdCdBr_3$ at 7 K.

		$A_\parallel$ (10^{-4} cm^{-1})		$A_\perp$ (10^{-4} cm^{-1})		
$\lvert g_\parallel \rvert$	$\lvert g_\perp \rvert$	^{171}Yb	^{173}Yb	^{171}Yb	^{173}Yb	J (10^{-4} cm^{-1})
2.503 ± 0.001	2.619 ± 0.001	666 ± 5	182 ± 0.5	708 ± 4	193.2 ± 0.5	-16 ± 2

or nearly coinciding with the two main central lines due to ^{even}Yb–V_{Cd}–^{even}Yb pairs, are not shown in the stick diagram of figure 1(b). It is interesting to note that the hyperfine patterns of the two pairs ^{171}Yb–V_{Cd}–^{even}Yb and ^{173}Yb–V_{Cd}–^{even}Yb have been fitted independently. The very good agreement of the ratio $(^{171}A_{\parallel}/^{173}A_{\parallel}) = (^{171}A_{\perp}/^{173}A_{\perp}) = 3.66$ with the theoretical value 3.63 of the ratio of g_N-values of the two isotopes provides a convincing argument for the validity of the simulation.

Besides the main EPR signals discussed so far, several very weak EPR lines are also observed (a few of these are indicated by stars in figures 1 and 2(a)). From their angular dependence which varies when $\boldsymbol{B}$ rotates in the a–b plane, it is evident that these weaker lines could be due to non-axial Yb^{3+} centres such as Yb^{3+}–(Cs^+ vacancy) with C_S symmetry. Due to the fact that such additional lines are also present in the half-field region (see figure 2(a)), it seems likely that these centres could also be non-axial Yb^{3+}–V_{Cd}–Yb^{3+} pairs with a defect in a neighbouring caesium site.

4. Discussion

4.1. Interionic separation and exchange interaction J

The excellent quality of the simulations (figures 1 and 2(b)) and the good agreement between the calculated and experimental angular variations for the line positions of the allowed $\Delta M_S = \pm 1$ transitions (figure 3) and for the intensity of the forbidden $\Delta M_S = \pm 2$ transitions (figure 2(b)) justify the use of Hamiltonian (3) for the description of Yb^{3+} pairs.

Let us first consider the magnetic dipolar spin–spin interaction, responsible for the separation $2(-2D_1 + D_2)$ between the two lines due to dominant pairs of even isotopes (see equation (6)). From the experimental weakly anisotropic g-values, listed in table 1, and using expressions for D_1 and D_2 from equation (5), the calculated magic angle (the angle θ at which dipolar splitting vanishes) comes out to be 53.63°, in close agreement with the experimental observation (figure 3) and the value 54.44° for the pure point dipole–dipole interaction between the two electronic spins with isotropic g-values. This provides confirmation that the use of a pure dipole–dipole expression in equation (3) is justified. Further, it follows from equation (5) that the dipolar splitting $2(-2D_1 + D_2)$ is simply $\beta^2(2g_{\parallel}^2 + g_{\perp}^2)/R^3$ for $\boldsymbol{B} \parallel \boldsymbol{c}$ and reduces to $\beta^2(2g_{\parallel}^2 + g_{\perp}^2)/2R^3$ for $\boldsymbol{B} \perp \boldsymbol{c}$. Thus, a reasonably accurate estimate of the distance R between the two Yb^{3+} ions in a pair can be made from the measured splittings. An interionic separation of 5.88 Å is calculated in this way. This distance is slightly smaller than that measured by Malkin *et al* [14]. It is, however, much smaller than the distance of 6.72 Å between two Cd^{2+} ions in second-neighbour positions in the host lattice. This indicates that there is a significant relaxation (about 12%) of Yb^{3+} ions towards the Cd^{2+} vacancy along the Yb^{3+}–V_{Cd}–Yb^{3+} axis (c-axis).

The other spin–spin interaction in Hamiltonian (3) is the isotropic exchange interaction J. Four allowed transitions at magnetic fields given by equation (9) are observed for each $m_1 = \langle I_z \rangle$ state, for pairs of the type ^{171}Yb–V_{Cd}–^{even}Yb and ^{173}Yb–V_{Cd}–^{even}Yb. The resonance lines corresponding to the subscripts 2 and 3 in equation (9) are observed at low fields while those corresponding to subscripts 1 and 4 appear at high fields. The energy separation between the adjacent transitions at B_2 and B_3 or B_1 and B_4, for a particular value of m_1, is $4D_1' = 4D_1 - 2J$. Further, the intensities of the allowed transitions for such pairs also depend on D_2' and thus on J. As the dipolar parameters D_1 and D_2 can be calculated from the g-values and the interionic distance R, the only unknown is the exchange interaction parameter J. Because of the large number of lines in the pair spectra of dissimilar ions, we were able to accurately determine the value of J. Moreover, changing the sign of J

modifies the appearance of the simulated spectra. Since the experimental spectra are well resolved, it was possible to determine the sign of J from simulation. The accuracy of the simulations precludes other contributions to V_{eff} and justifies the use of just isotropic exchange and magnetic dipolar interactions in expression (2). Negligible admixtures from various other exchange mechanisms, involving orbital angular momentum operators and giving other anisotropic terms, are evident from the weakly anisotropic g-factors, relatively close to the free-spin g-value, so the situation is similar to that of a quenched orbital momentum.

From the experimental value $J = -16 \times 10^{-4}$ cm^{-1}, it follows that the exchange coupling between the two Yb^{3+} ions of a pair is antiferromagnetic but extremely weak. It is of the same order of magnitude as the value $J = -6 \times 10^{-4}$ cm^{-1} measured for Gd^{3+}–Gd^{3+} pairs in $CsCdBr_3$ [4]. This very small value of J is also evident from the number of resonance lines observed in the EPR spectra of dissimilar ions. In the weak-exchange limit, the singlet and triplet states do not constitute pure spin states, so all four states are retained in the calculations [18]. In other words, singlet–triplet transitions are not forbidden and $4(2I + 1)$ allowed $\Delta M_S = \pm 1$ transitions are expected, as observed experimentally.

The fact that the resulting exchange energy is weak does not necessarily mean that such contributions are negligible in the ion–ion interaction. J is generally the sum of a positive, through space, contribution of the ferromagnetic type, $J_F > 0$, and a negative antiferromagnetic contribution, $J_{AF} < 0$, due to superexchange: $J = J_F + J_{AF}$. Ferromagnetic interactions of the order of a cm^{-1} cannot be definitely excluded since they seem to contribute to the optical spectra of Nd^{3+} in YVO_4, $YLiF_4$ and possibly YAG matrices [15]. A superexchange interaction J_{AF} of the same order of magnitude as J_F could thus result in a very small effective exchange energy J. The interpretation of the optical spectra of Yb^{3+} in $CsCdBr_3$ by Malkin *et al* [14], based on a configuration interaction between the ground state $4f^{13}(Yb^{3+})[4p^6(Br^-)]_6$ and excited state $4f^{14}(Yb^{3+})4p^5(Br)[4p^6(Br^-)]_5$ configurations, provides an argument in favour of antiferromagnetic interaction between Yb^{3+} ions, as these covalency effects are known to mediate the superexchange interaction [18]. ENDOR spectroscopy should thus be able to give more information about Br^-Yb^{3+} covalency, and thus about superexchange.

4.2. Electronic ground state

The experimental g-values can be used to determine the structure of the ground-state Kramers doublet of Yb^{3+} in $CsCdBr_3$. In cubic symmetry, the g-factor depends on the coordination of the Yb^{3+} ion. For sixfold coordination (octahedral site), the predicted ground state is the Γ_6 doublet, with a theoretical g-value $g_{cub} = -2.663$, while Γ_7 is the ground-state doublet for twelvefold coordination with $g_{cub} = -3.428$. When the distortion from cubic to lower symmetry is small in comparison with the cubic crystal field, the average g-factor, $\tilde{g} = \frac{1}{3}(g_x + g_y + g_z)$, is expected to be close to g_{cub} [19]. Owing to the basically octahedral coordination of Yb^{3+} in $CsCdBr_3$, we may use this rule to deduce the signs of $g_\parallel$ and $g_\perp$, which are not known from the experimental spectra. We obtain $\tilde{g} = -2.580$ for $g_\parallel, g_\perp < 0$ and $|\tilde{g}| = 0.912$ if $g_\parallel$ and $g_\perp$ have opposite signs. Comparison with the theoretical value $g_{cub} = -2.663$ for octahedral symmetry indicates unambiguously that $g_\parallel$ and $g_\perp$ are both negative. In a crystal field of trigonal symmetry, the Γ_6 doublet of pure octahedral symmetry becomes the Γ_4 doublet, which displays the following structure:

$$|\Gamma_4, \mp\rangle = \pm a \left|\frac{7}{2}, \pm\frac{1}{2}\right\rangle \pm b \left|\frac{7}{2}, \pm\frac{7}{2}\right\rangle \mp c \left|\frac{7}{2}, \mp\frac{5}{2}\right\rangle. \tag{12}$$

Here the states are written in $\{|J, M_J\rangle\}$ representation, $M_J = J, J-1, \ldots, -J$ being the z-projection of $J = -7/2$, and the $\mp$ sign in $|\Gamma_4, \mp\rangle$ refers to the $\mp 1/2$ values of the

single-hole spin of the f^{13} configuration. In expression (12) we have neglected admixture of excited $J = 5/2$ states, which agrees with the fact that the ratio $|g_\perp A_\parallel / g_\parallel A_\perp| = 0.984$ for ^{171}Yb and 0.986 for ^{173}Yb is close to one, as expected for a pure $J = 7/2$ state [20]. The parallel and perpendicular components of the g-factor derived from the $|\Gamma_4, \mp\rangle$ state are the following:

$$g_\parallel = g_J(-a^2 - 7b^2 + 5c^2) \tag{13a}$$

and

$$g_\perp = g_J(+4a^2 - 2\sqrt{7}bc) \tag{13b}$$

where $g_J = 8/7$ is the Landé factor for the $^2F_{7/2}$ level of Yb^{3+}. Solving equations (13), we get the following set of values: $a^2 = 0.045$, $b^2 = 0.5767$ and $c^2 = 0.3783$ for the normalized coefficients which give the experimental g-values. The ground state of Yb^{3+} in $CsCdBr_3$ is thus essentially made up of $|M_J| = 7/2$ and $5/2$ states with a very small admixture of the $|M_J| = 1/2$ states.

It can be useful to describe the ground state in the usual f-orbital representation. In this case the wave function given by equation (12) in $\{|J, M_J\rangle\}$ representation is transformed to the $\{|L = 3, S = \frac{1}{2}, M_L, M_S\rangle\} \equiv \{|M_L, M_S\rangle\}$ representation (M_L is the projection of the orbital angular momentum L on the z-axis) as

$$|\pm\rangle = p\left|\pm 0, \pm\frac{1}{2}\right\rangle + q\left|\pm 1, \mp\frac{1}{2}\right\rangle + r\left|\mp 2, \mp\frac{1}{2}\right\rangle + s\left|\pm 3, \pm\frac{1}{2}\right\rangle + t\left|\mp 3, \pm\frac{1}{2}\right\rangle \tag{14}$$

where $M_L = 0$, 1, 2 and 3 represent f_σ, f_π, f_δ and f_ϕ orbitals, respectively. The coefficients p, q, r, s and t can be obtained from a, b and c by using the expansions

$$|J, M_J\rangle = \sum_{M_L, M_S} \langle M_L, M_S | J, M_J\rangle |M_L, M_S\rangle |M_L M_S\rangle$$

where $\langle M_L, M_S | J, M_J\rangle$ are the Clebsch–Gordan coefficients [21]. This gives

$$\begin{aligned} p^2 &= \frac{4}{7}a^2 = 0.0257 \qquad & q^2 &= \frac{3}{7}a^2 = 0.0193 \qquad & r^2 &= \frac{6}{7}c^2 = 0.3243 \\ s^2 &= b^2 = 0.5767 \qquad & t^2 &= \frac{1}{7}c^2 = 0.0540. \end{aligned} \tag{15}$$

Thus the ground-state orbital is mainly composed of $4f_\phi$ (63.1%) and $4f_\delta$ (32.4%) orbitals, with very small contributions from $4f_\pi$ and $4f_\sigma$ orbitals.

5. Conclusions

More than 95% of the Yb^{3+} ions in $CsCdBr_3$:1.3% Yb sample form weakly antiferromagnetically coupled symmetric Yb^{3+}–V_{Cd}–Yb^{3+} pair complexes. The present studies also show the existence of perturbed Yb^{3+} sites of lower symmetry in very small proportions. It is important to note that there are no asymmetric pair complexes of the type Yb^{3+}–Yb^{3+}–V_{Cd}. The hysteresis of near-infrared and cooperative upconversion luminescence as a function of incident laser intensity has been observed exclusively for excitation of the optical line at about 2 cm^{-1} above the main absorption line of Yb^{3+}–V_{Cd}–Yb^{3+} centres in $^2F_{7/2}(0) \rightarrow {}^2F_{5/2}(2')$ luminescence excitation spectra [3]. This relatively intense line was previously attributed to Yb^{3+}–Yb^{3+}–V_{Cd} asymmetric pairs [3], which now appears unlikely on the basis of the present EPR experiments.

Acknowledgments

The authors are grateful to Mrs D Simmons for technical assistance and Dr F Pellé for providing the Yb:$CsCdBr_3$ crystals used in this work.

References

[1] Hehlen M P, Güdel H U, Shu Q, Rai J, Rai S and Rand S C 1994 *Phys. Rev. Lett.* **73** 1103
[2] Lüthi S R, Hehlen M P, Riedener T and Güdel H U 1998 *J. Lumin.* **76+77** 447
[3] Hehlen M P, Kuditcher A, Rand S C and Lüthi S 1999 *Phys. Rev. Lett.* **82** 3050
[4] McPherson G L and Henling L M 1977 *Phys. Rev.* B **16** 1889
Henling L M and McPherson G L 1977 *Phys. Rev.* B **16** 4756
[5] McPherson G L and Devaney K O 1980 *J. Phys. C: Solid State Phys.* **13** 1735
[6] Barthou C and Barthem R B 1990 *J. Lumin.* **46** 9
[7] Goldner Ph and Pellé F 1993 *J. Lumin.* **55** 197
[8] Neukum J, Bodenschatz N and Heber J 1994 *Phys. Rev.* B **50** 3536
[9] Pellé F, Goldner Ph and Pilla O 1993 *J. Phys.: Condens. Matter* **5** 3381
[10] Mujaji M, Jones G D and Syme R W G 1993 *Phys. Rev.* B **48** 710
[11] Pellé F, Gardant N, Genotelle M, Goldner Ph and Porcher P 1995 *J. Phys. Chem. Solids* **56** 1003
[12] Murdoch K M and Cockroft N J 1996 *Phys. Rev.* B **54** 4589
[13] Heber J, Lange M, Altwein M, Malkin B Z and Rodionova M P 1998 *J. Alloys Compounds* **275–277** 181
[14] Malkin B Z, Leushin A M, Iskhakova A I, Heber J, Altwein M, Moller K, Fazlizhanov I I and Ulanov V A 2000 *Phys. Rev.* B **62** 7063
[15] Guillot-Noël O, Mehta V, Viana B, Gourier D, Boukhris M and Jandl S 2000 *Phys. Rev.* B **61** 15 338
[16] Cone R L and Meltzer R S 1987 *Spectroscopy of Solids Containing Rare Earth Ions* (Amsterdam: North-Holland–Elsevier Science)
[17] Baker J M 1971 *Rep. Prog. Phys.* **34** 109
[18] Bencini A and Gatteschi D 1989 *EPR of Exchange Coupled Systems* (Berlin: Springer)
[19] Lewis H R and Sabinsky E S 1963 *Phys. Rev.* B **130** 1370
[20] Abragam A and Bleaney B 1970 *Electron Paramagnetic Resonance of Transition Ions* (Oxford: Oxford University Press)
[21] Brandsen B H and Joachain C J 1995 *Introduction to Quantum Mechanics* (New York: Wiley)